

Magnetic and electronic properties of La-doped hexagonal 4H-$SrMnO_3$

Jie Li(李杰), Yinan Chen(陈一楠), Nuo Gong(宫诺), Xin Huang(黄欣), Zhihong Yang(杨志红), and Yakui Weng(翁亚奎)

Citation: Chin. Phys. B, 2024, 33 (**1**): 017502. DOI: 10.1088/1674-1056/acf995

Journal homepage: http://cpb.iphy.ac.cn; http://iopscience.iop.org/cpb

What follows is a list of articles you may be interested in

Review of photoinduced effect in manganite films and their heterostructures

Xin-Yu Li(李欣谕), Long Zhao(赵龙), Xiang-Yang Wei(魏向洋), Hao Li(李豪), Ke-Xin Jin(金克新)

Chin. Phys. B, 2018, 27 (**11**): 117501. DOI: 10.1088/1674-1056/27/11/117501

Room-temperature ferromagnetism observed in Nd-doped In_2O_3 dilute magnetic semiconducting nanowires

Zhanpeng Lv(吕占朋), Junran Zhang(张军然), Wei Niu(钮伟), Minhao Zhang(张敏昊), Li Song(宋丽), Hairong Zhu(朱海荣), Xuefeng Wang(王学锋)

Chin. Phys. B, 2016, 25 (**9**): 097502. DOI: 10.1088/1674-1056/25/9/097502

Nanoscale control of low-dimensional spin structures in manganites

Jing Wang(王静), Iftikhar Ahmed Malik, Renrong Liang(梁仁荣), Wen Huang(黄文), Renkui Zheng(郑仁奎), Jinxing Zhang(张金星)

Chin. Phys. B, 2016, 25 (**6**): 067504. DOI: 10.1088/1674-1056/25/6/067504

Structural and magnetic properties of $La_{0.7}Sr_{0.1}Ag_xMnO_{3-\delta}$ perovskite manganites

Hou Xue (侯雪), Ji Deng-Hui (纪登辉), Qi Wei-Hua (齐伟华), Tang Gui-De (唐贵德), Li Zhuang-Zhi (李壮志)

Chin. Phys. B, 2015, 24 (**5**): 057501. DOI: 10.1088/1674-1056/24/5/057501

Colossal magnetoresistance in manganites and related prototype devices

Liu Yu-Kuai (刘愉快), Yin Yue-Wei (殷月伟), Li Xiao-Guang (李晓光)

Chin. Phys. B, 2013, 22 (**8**): 087502. DOI: 10.1088/1674-1056/22/8/087502

Magnetic and electronic properties of La-doped hexagonal 4H-$SrMnO_3$

Jie Li(李杰)[1], Yinan Chen(陈一楠)[2], Nuo Gong(宫诺)[2], Xin Huang(黄欣)[2], Zhihong Yang(杨志红)[2], and Yakui Weng(翁亚奎)[2,†]

[1] *Grünberg Research Centre, Nanjing University of Posts and Telecommunications, Nanjing* 210023, *China*
[2] *School of Science, Nanjing University of Posts and Telecommunications, Nanjing* 210023, *China*

(Received 19 June 2023; revised manuscript received 28 August 2023; accepted manuscript online 14 September 2023)

As typical strongly correlated electronic materials, manganites show rich magnetic phase diagrams and electronic structures depending on the doped carrier density. Most previous relevant studies of doped manganites rely on the cubic/orthorhombic structures, while the hexagonal structure is much less studied. Here first-principles calculations are employed to investigate the magnetic and electronic structures of La-doped 4H-$SrMnO_3$. By systematically analyzing the two kinds of La-doped positions, our calculations predict that the doped electron with lattice distortion would prefer to form polarons, which contribute to the local magnetic phase transition, nonzero net magnetization, and semiconducting behavior. In addition, the energy gap decreases gradually with increasing doping concentration, indicating a tendency of insulator–metal transition.

Keywords: manganites, polaron, magnetic phase transition

PACS: 75.47.Lx, 71.30.+h, 71.38.–k **DOI:** 10.1088/1674-1056/acf995

1. Introduction

Tuning magnetic and electronic states in materials is one of the fundamental goals for both basic science and practical applications.[1–3] To achieve this goal, two conditions need to be met: (i) effective modulation method, and (ii) ideal material platform. Firstly, in terms of regulation methods, a frequently used approach is doping, which can be realized through oxygen deficiency,[4–6] cation substitution,[7–10] and interfacial charge transfer.[11–14] Via proper doping, one can engineer exciting physical phenomena in a new dimension,[15,16] such as magnetic phase transition and insulator–metal transition (or even insulator–superconductor transition).[17,18]

Secondly, in terms of material platform, transition metal oxides have been providing a fertile ground for studying novel functionalities and relevant physics, since they not only have vast family members (from 3d to 4d/5d systems) with various structures, but also possess fascinating physical phenomena due to the multiple physical couplings among various degrees of freedom (spin, charge, orbital and lattice).[19–21] Among these focused materials, Mn-based oxides have attracted enormous attention and been extensively studied for their rich magnetic phase diagrams, colossal magnetoresistivity, and multiferroicity.[19,22,23]

$SrMnO_3$ (SMO) is a rare example of compounds that has both cubic structure and hexagonal (4H) structures,[24] which are antiferromagnetic insulators with Néel temperatures of ~ 233 K and ~ 280 K, respectively.[25–27] Since the tolerance factor t is larger than 1 ($t = 1.04$), 4H-SMO [see Fig. 1(a)] is normally stable under ambient conditions, whereas the cubic phase is commonly observed in a metastable state.[28–30] In comparison of the hexagonal SMO with the cubic SMO, it can be found that their crystal structures are completely different. Cubic SMO contains only corner-sharing octahedra, while 4H-SMO structure contains both corner- and face-sharing octahedra [see Fig. 1(a)]. In addition, their spin arrangements are different, although both of them are in antiferromagnetic background. Cubic SMO is G-type antiferromagnetic ordering, while spin arrangement of 4H-SMO is in layered form, similar to the A-type antiferromagnetic ordering. Therefore, considering the rich electronic and magnetic properties presented in doped cubic structure, it is worthwhile to study the doped 4H structure.

However, most of the previous experimental studies have been focused on the metastable cubic SMO with low and high electron doping,[31,32] while the physical properties of carrier doped-4H SMO has rarely been studied. The only recent report on electron doping of 4H-SMO is fluorinated hexagonal SMO (i.e., $SMO_{3-x}F_x$).[33] Although some interesting properties (i.e., a spin- or cluster-glass-like state and ferroelectric nature) have been observed in such F-doped 4H-SMO, more exciting physical properties, such as magnetic phase transition, insulator-to-metal transition and magnetic polaron, remain unexplored in 4H-SMO.

In general, doping of Mn-based oxides is usually achieved by introducing rare-earth (or alkaline-earth) cations rather than anions into the host material, which can be expressed as $R_{1-x}A_xMnO_3$ (or $A_{1-x}R_xMnO_3$), where R and A are rare- and alkaline-earth cations, respectively. Therefore, in this work,

†Corresponding author. E-mail: wyk@njupt.edu.cn

© 2024 Chinese Physical Society and IOP Publishing Ltd

we perform systematic first-principles calculations to study the magnetic and electronic properties of doped 4H-SMO by using La^{3+} to replace Sr^{2+} [i.e., 4H-$La_xSr_{1-x}MnO_3$ (LSMO)]. Due to the formation of magnetic polaron, the doped 4H-SMO undergoes a localized magnetic phase transition from antiferromagnetism to ferrimagnetism. In addition, the energy gap decreases gradually with increasing doping concentration, exhibiting a tendency toward an insulator-to-metal transition.

2. Model and method

The following calculations were performed using the projector augmented wave pseudopotentials as implemented in the Vienna *ab initio* simulation package (VASP) code.[34,35] The revised Perdew–Burke–Ernzerhof for solids functional and the generalized gradient approximation (GGA) method are adopted to describe the crystalline structure and electron correlation.[36] The cutoff energy of plane wave is 550 eV. For both SMO and LSMO ($x = 0.25$), a $9 \times 9 \times 5$ Monkhorst–Pack k-point mesh centered at the Γ point is adopted for the Brillouin-zone integrations, while $9 \times 9 \times 3$ and $10 \times 10 \times 2$ meshes are used for $x = 0.125$ and $x = 0.083$ cases, respectively.

The unit cell of 4H-SMO structure has 20 atoms (4 f.u.). Starting from the experimental 4H structure (space group $P6_3/mmc$, $a = 5.4434$ Å and $c = 9.0704$ Å),[26] the lattice constants and inner atomic positions are fully relaxed until the Hellman–Feynman forces are converged to less than 0.01 eV/Å. Using the Dudarev implementation,[37] various values of the Hubbard repulsion U_{eff} ($= U - J$) on Mn 3d orbitals have been tested from 0 eV to 2 eV. For bulk 4H-SMO, both GGA and GGA $+U$ can give reasonable crystal structure parameters (within <1% deviation) and well reproduce the magnetic ground state. To better compare with the data calculated by pure GGA in the literature,[28,38] the GGA is also adopted in this work, if it is not noted explicitly.

3. Results and discussion

Undoped SMO As shown in Fig. 1(a), 4H-SMO structure (space group $P6_3/mmc$) contains both corner- and face-sharing octahedra, which is different from the cubic SMO with corner-sharing octahedra only. This hexagonal structure has relatively shorter Mn–Mn bonds with face sharing, resulting in Mn_2O_9 dimers, while relatively longer Mn–Mn bonds are shown with corner sharing.

First, to determine the magnetic ground state of undoped 4H-SMO, four most possible magnetic orders: ferromagnetism (FM), type-I antiferromagnetism (AF1), type-Ⅱ antiferromagnetism (AF2) and type-Ⅲ antiferromagnetism (AF3) [see Fig. 1(b)] are calculated and compared in energy. Taking the AF1 state (all Mn ions are antiferromagnetically coupled along the c-axis) as the energy reference, the energies of all magnetic orders are summarized in Table 1, which suggest the AF1 to be the most stable state, in agreement with the previous studies.[28,39] In addition, according to these energy differences among various magnetic orders, the exchange coefficients can be obtained by mapping the system to a classical spin model with normalized spins ($|S| = 1$). Here, the nearest-neighbor exchange J_1 refers to the magnetic coupling between face-shared Mn ions, while the next-nearest-neighbor exchange J_2 refers to the magnetic coupling between corner-shared Mn ions, as indicated in Fig. 1(b). For undoped 4H-SMO, J_1 and J_2 are 36.1 meV and 51.0 meV (see Table 1), respectively, implying a strong AFM coupling between Mn ions.

Table 1. Comparison of undoped SMO and LSMO ($x = 0.25$). The energy difference (in units of meV/Mn), exchange coefficients (in units of meV) and net magnetization (in units of μ_B) are from DFT calculations. AF1 is taken as the reference state for energy comparison. Exchange coefficients (nearest-neighbor exchange J_1 and next-nearest-neighbor exchange J_2) are calculated by mapping the DFT energies. Pure electron concentration (ele-concentration) case and pure lattice distortion case are also tested and compared. Notably, for the cases of $x = 0.25$ (case B) and pure ele-concentration, while 'AF2' is ferrimagnetic, it has the same spin arrangement as AF2 order [see Fig. 2(b)].

	AF1	AF2	AF3	FM	J_1	J_2	M
Undoped SMO	0	36.1	153.0	203.6	36.1	51.0	0
$x = 0.25$ (case A)	0	−12.8	16.7	52.6	−12.8	5.6	0
$x = 0.25$ (case B)	0	−66.1	13.1	27.3	−66.1	4.4	−1
Pure ele-concentration	0	−39.0	20.5	30.1	−39.0	6.8	−0.87
Pure lattice distortion	0	56.9	139.1	214.2	56.9	46.4	0

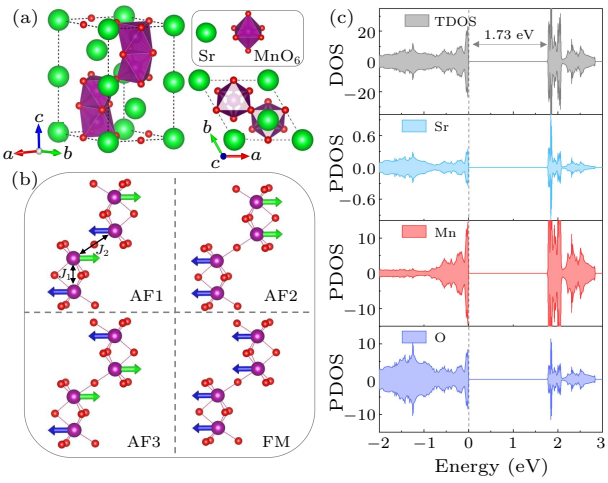


Fig. 1. (a) The side view and top view of 4H-SMO unit cell. Corner- and face-sharing octahedra are seen along the c axis. (b) Schematics of four possible magnetic orders: type-I antiferromagnetism (AF1), type-Ⅱ antiferromagnetism (AF2), type-Ⅲ antiferromagnetism (AF3), and ferromagnetism (FM). Exchange couplings are also indicated: nearest-neighbor exchange J_1 and next-nearest-neighbor exchange J_2. (c) The density of states (DOS) and atom projected DOS (PDOS) of 4H-$SrMnO_3$ near the Fermi level. The Fermi energy is located at zero.

Second, the total density of states (DOS) and atomic-projected density of states (PDOS) of 4H-SMO are shown in Fig. 1(c). Clearly, the system is a Mott insulator with energy gap of ∼ 1.74 eV, even in the pure GGA calculation,

which agrees with the previous calculations.[28,38] The calculated magnetic moment is 2.45 μ_B/Mn, implying the high-spin state of Mn^{4+} (d^3 configuration). Both the valance band maximum and the conduction band minimum are mainly contributed by Mn t_{2g} orbitals, despite the presence of hybridization between Mn 3d and O 2p orbitals around the Fermi level.

In our DFT calculation with spin-orbit coupling (SOC), the energy of spins parallel to the *xy* plane is slightly lower ($\sim$ 0.15 meV/u.c.) than the energy of spins along the *c*-axis, in agreement with the previous study.[28] However, compared with the results without SOC effect, the energy gap and magnetic moment with SOC are almost unchanged (i.e., $\sim$ 1.73 eV and 2.44 μ_B/Mn, respectively), implying that the influence of SOC effect is very weak in this system and can be ignored in the following calculations.

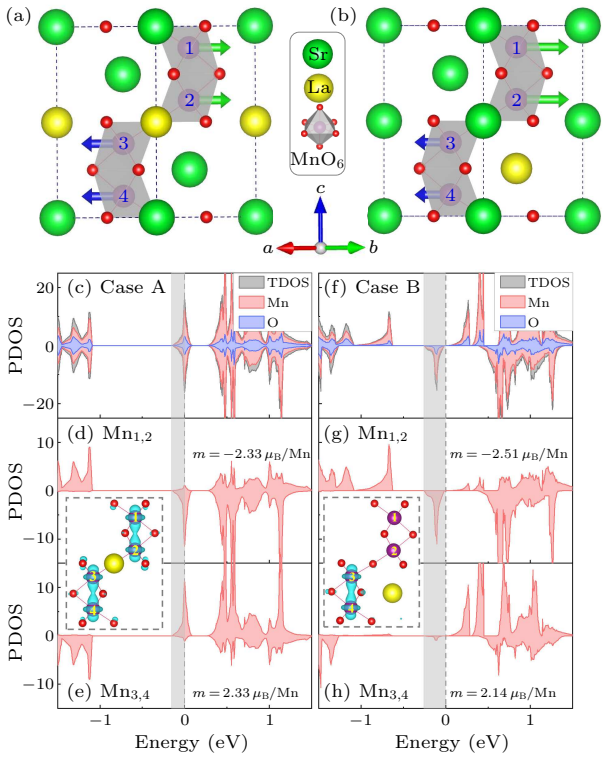


Fig. 2. Crystal structure and corresponding electronic structure of La-doped SMO. [(a), (b)] Two kinds of La-doped structures: (a) case A, (b) case B. The direction and length of the arrows indicate different spin arrangements and magnetic moments, respectively. Obviously, case A is antiferromagnetic, while case B is ferrimagnetic with the same spin arrangement as AF2 order. (c)–(h) Density of state (DOS) and projected density of state (PDOS) of La-doped SMO: (c)–(e) case A; (f)–(h) case B. The Fermi level for each case is set as zero, and the local moments of Mn ions are indicated. The portion of the valence band associated with electron doping is shaded in gray. Inset: the corresponding spatial distribution of added electron in La-doped SMO.

La-Doped SMO First, the theoretically simplest doping case, i.e., 25% doping, is studied by using one La to replace one Sr in a unit cell. Due to the different valences between La^{3+} and Sr^{2+}, one more electron will be introduced into the system, which can effectively modulate the magnetic order and electronic structure. Since there are two kinds of nonequivalent La atoms in the 4H-SMO system, two doping cases (case A and case B) are tested and compared, as shown in Figs. 2(a) and 2(b).

In our calculations, the crystal structures of La-doped SMO are re-optimized with varying magnetism. As summarized in Table 1, the total energies show that AF2 is the most stable state for both cases A and B, instead of original AF1 in pure SMO bulk, suggesting the doping-driven magnetic phase transition. Interestingly, the intrinsic physical properties of cases A and B are completely different, even though both of them exhibit magnetic phase transitions:

(i) The magnetic coupling strengths are different. For case A, the values of both J_1 and J_2 are significantly reduced compared with those of the pure SMO. For case B, although the values of J_2 is still smaller than that of the pure SMO, the magnitude of its J_1 is nearly twice as large as that of the pure SMO (see Table 1).

(ii) The net magnetic moments are different. The net magnetization of case A is 0 μ_B/u.c., indicating that the system remains antiferromagnetism. However, the net magnetization of case B is -1 μ_B/u.c. In this case, case B should be ferrimagnetic (with the same spin arrangement as AF2 order) rather than antiferromagnetic (see Table 1).

(iii) The electronic structures are different. As shown in Figs. 2(c) and 2(f), case A becomes metallic and undergoes an insulator–metal transition, while the energy gap of case B still exists despite very small value ($\sim$ 0.07 meV).

To understand what makes case A different from case B, the atomic-projected density of states (PDOS) and corresponding distribution of electrons are plotted, which can be qualitatively used to analyze the effect of added electron on electronic structure, orbital occupation, and magnetic moment. As shown in Fig. 2(a), since the doped La in case A is occupies a highly symmetric position, the introduced electron is equally divided by all Mn ions, which can be visualized by PDOS, local magnetic moments, as well as the spatial distribution of electron [see Figs. 2(d) and 2(e)]. In this case, all Mn ions within antiferromagnetic order are partially occupied, leading to a metallic behavior and zero net magnetic moment.

However, for case B, the position of doped La ion is no longer located in the center of the two Mn_2O_9 dimers but close to one of them (i.e., Mn_3–Mn_4 dimer) [see Fig. 2(b)], then the occupation of the introduced electron on the near-La dimer (i.e., Mn_3–Mn_4 dimer) is more prominent than that of the other one (i.e., Mn_1–Mn_2 dimer). As shown in Figs. 2(g) and 2(h), the added electron is indeed localized on Mn_3–Mn_4 dimer, resulting in an uneven distribution of charges and unequal local magnetic moments between the Mn_3–Mn_4 (2.14 μ_B/Mn) and Mn_1–Mn_2 (-2.51 μ_B/Mn) dimers. In addition, compared with the Mn–O–Mn bond angles ($\sim$ 80.9°) in bulk 4H-SMO, the change of Mn–O–Mn bond angles in the Mn_3-Mn_4 dimer ($\sim$ 76.9°) is relatively large, whereas the change of Mn–O–

Mn bond angles in the Mn_1–Mn_2 dimer ($\sim 81.1^\circ$) is very small. Considering the results of electron restricted by strong Coulombic interaction and the lattice distortions in this system, the 3d polaron is formed, which will enhance the nearest-neighbor magnetic coupling and contribute to the semiconductor behavior.[9] Similar magnetic polarons also exist in the electron-doped manganite $La_xCa_{1-x}MnO_3$, which are Mn-sites FM clusters embedded in AFM region.[40] Based on the polaron forming and antiferromagnetic arrangement between Mn_3–Mn_4 dimer and Mn_1–Mn_2 dimer, a nonzero net magnetic moment appears.

By comparing the energies of cases A and B, it is found that case B owns the lowest energy ($\sim$ 109 meV/Mn lower than that of case A), indicating that it is easier to form magnetic polaron in the La-doped 4H-SMO structure. The underlying physical mechanism is that the 3d electrons have strong Hubbard interaction, which tend to favor localized magnetic moments, thus the energy gain from forming magnetic polaron is larger than that of delocalized one.[40] In the following calculation, case B is adopted as default doped structure.

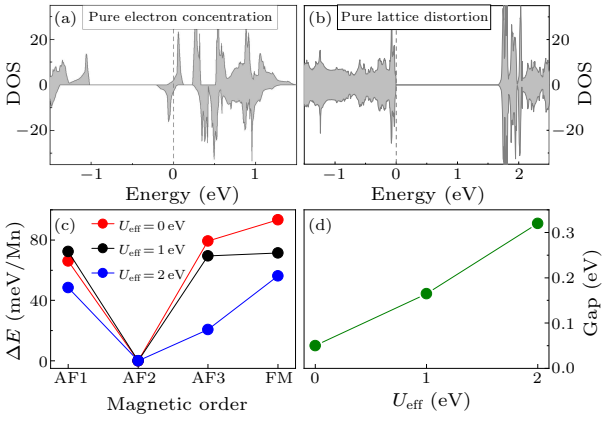


Fig. 3. The tested magnetic and electronic properties of case B. (a) Electronic structure with only pure electron concentration. The Fermi energy is positioned at zero. (b) Electronic structure with only pure lattice distortion. (c) The energy difference as a function of $U_{\rm eff}$. Here, AF2 is taken as the reference state for energy comparison. (d) The energy gap as a function of $U_{\rm eff}$.

As discussed above, the chemical doping effect on the material is usually achieved by changing both carrier concentration and lattice distortion. A direct question is which factor dominates the magnetic phase transition and which factor dominates the change in electronic structure, or both together. To clarify the physical mechanisms behind these phenomena, pure electron concentration and pure lattice distortion are calculated. Here, the pure electron concentration is simulated by embedding La ion in the ground-state SMO structure without re-optimizing the lattice structure, thus qualitatively avoiding the effect of lattice distortion. In contrast, the pure lattice distortion is achieved by calculating pure SMO with the same structure as the ground-state LSMO, so the system maintains the same electron concentration as pure SMO and retains the same lattice distortion generated by La doping.

As listed in Table 1, the magnetic phase transition from AF1 to AF2 and a net magnetic moment can be induced by pure electron concentration but not by pure lattice distortion, implying that the magnetic properties of La-doped SMO are mainly affected by electron concentration. However, the net magnetic moment induced by pure electron concentration ($-0.87\mu_B$) is slightly smaller than that of the real system with lattice distortion ($-1\mu_B$). The underlying reason for this issue is that in the absence of lattice distortion, the doped electron is slightly diffused and not completely localized on the near-La Mn dimer, leading to metallic behavior [see Fig. 3(a)] and reduction of the net magnetic moment (see Table 1). By considering lattice distortion but without alteration of electron concentration, the energy gap is almost the same as that of pure SMO, as shown in Fig. 3(b). Therefore, the semiconducting behavior and $-1\mu_B$ net moment are the result of a cooperative mechanism between electron concentration and lattice distortion.

To further verify the reliability of the magnetic phase transition, the energy difference is also calculated by varying $U_{\rm eff}$. As shown in Fig. 3(c), taking AF2 as the reference state for energy comparison, the energy differences are always positive, implying a robust conclusion for the magnetic phase transition in La-doped SMO. The energy gap is also checked, as shown in Fig. 3(d). The energy gap increases almost linearly with $U_{\rm eff}$, suggesting a semiconductor fact for La-doped SMO.

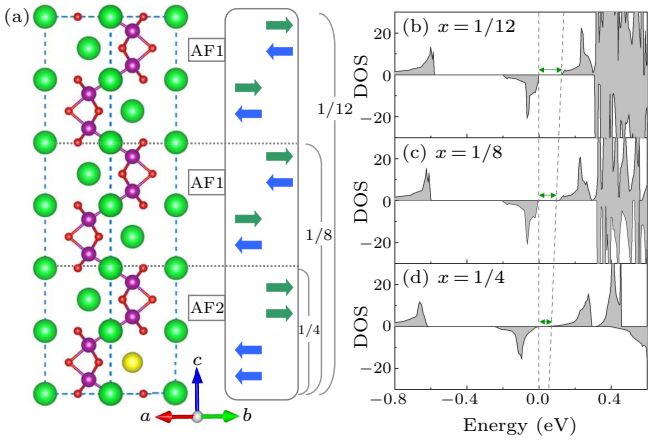


Fig. 4. (a) Left: crystalline structure of $La_xSr_{1-x}MnO_3$ along the c axis with different doping concentrations: 25% ($x=1/4$), 12.5% ($x=1/8$), and 8.25% ($x=1/12$). Green: Sr; yellow: La; purple: Mn; red: O. Right: the corresponding magnetic ground states: AF2 for $x=1/4$, AF2–AF1 hybrid magnetic order for $x=1/8$ and $x=1/12$. (b)–(d) DOS near the Fermi level plotted with some selected doping concentrations: 25%, 12.5%, and 8.25%. The Fermi energy is located at zero. The topmost valence band and the bottommost conducting band are marked by (gray) broken lines.

The localization of added electron can be further confirmed by calculating other doping concentrations (i.e., $x=1/8$ and $x=1/12$), as shown in Fig. 4. Starting from the $x=1/4$ minimal cell, pure SMO cell is doubled/trebled along the c axis. To determine the magnetic ground state, several possible magnetic orders have been tested, including FM,

AF1, AF2, AF3, and a special hybrid magnetic order [denoted as AF2–AF1 here; see Fig. 4(a)]. The AF2–AF1 state is AF2 order in the La-doped unit cell but AF1 order in La-undoped unit cell (or supercells).

In our calculations, the AF2–AF1 state owns the lowest energy for both $x = 1/8$ and $x = 1/12$ cases, due to the formation of magnetic polaron. Such a magnetic polaron can be further confirmed by the total DOS. As shown in Fig. 4(b), the electron-occupied or even unoccupied states (near the Fermi level) in $x = 1/8$ and $x = 1/12$ cases are very similar to the $x = 1/4$ case, suggesting the same localized feature of electronic structures. In addition, with decreasing doping concentration, the reduced doping/undoping ratio will make the energy gap approach to the pure SMO, leading to a gradually increasing bandgap. In other words, the energy gap decreases with increasing doping concentration until the highly probable insulator–metal transition occurs. Of course, in DFT calculation with high-density electron doping, there are many choices for the design of doping structure (ordered or disordered), so the final electronic properties may also change accordingly, which need further experimental confirmation and verification.

4. Conclusion

In summary, magnetic and electronic properties of La-doped 4H-SMO have been studied systematically using the first-principles calculation. The La doping to 4H-SMO can not only modulate the electron concentration but also affect the lattice distortion. The extra electron with distorted lattice forms the polaron, leading to a localized magnetic phase transition from antiferromagnetism to ferrimagnetism as well as the semiconducting behavior. Moreover, with increasing doping concentration, the energy gap of La-doped 4H-SMO decreases gradually, showing a tendency of insulator-to-metal transition. Further experimental studies are expected to confirm and verify our predictions.

Acknowledgment

This work was supported by the Natural Science Foundation of Nanjing University of Posts and Telecommunications (Grant Nos. NY222167 and NY220005).

References

[1] Dagotto E and Tokura Y 2008 *MRS Bull.* **33** 1037
[2] Dong S, Xiang H J and Dagotto E 2019 *Natl. Sci. Rev.* **6** 629
[3] Chakhalian J, Freeland J W, Millis A J, Panagopoulos C and Rondinelli J M 2014 *Rev. Mod. Phys.* **86** 1189
[4] Zhang Q, He X, Shi J, Lu N, Li H, Yu Q, Zhang Z, Chen L Q, Morris B, Xu Q, Yu P, Gu L, Jin K and Nan C W 2017 *Nat. Commun.* **8** 104
[5] An M, Weng Y K, Zhang H M, Zhang J J, Zhang Y and Dong S 2017 *Phys. Rev. B* **96** 235112
[6] Espinosa-García W F and Dalpian G M 2021 *Phys. Rev. B* **104** 205106
[7] Iglesias L, Bibes M and Varignon J 2021 *Phys. Rev. B* **104** 035123
[8] Li W, Dong S, Fang C and Hu J P 2012 *Phys. Rev. B* **85** 100407
[9] Gao B, Weng Y K, Zhang J J, Zhang H M, Zhang Y and Dong S 2017 *J. Phys.: Condens. Matter* **29** 095803
[10] Hao J J, Sun P H, Zhang M, Wu X X, Liu K and Yang F 2022 *Chin. Phys. Lett.* **39** 067402
[11] Zhong Z C and Hansmann P 2017 *Phys. Rev. X* **7** 011023
[12] Shen M L, Weng Y K, Yi Y W, Geng Q F, Yan W, Wang H Y, Yang J P and Li X 2019 *J. Appl. Phys.* **126** 085307
[13] Weng Y K, Shen M L, Li J and Li X A 2020 *Chin. Phys. B* **29** 127303
[14] Weng Y K, Long F, Chen Y N, Miao F Y, Li J, Cheng J and Li X 2023 *J. Appl. Phys.* **133** 235301
[15] Lee P A, Nagaosa N and Wen X G 2006 *Rev. Mod. Phys.* **78** 17
[16] Li D F, Lee K, Wang B Y, Osada M, Crossley S, Lee H R, Cui Y, Hikita Y and Hwang H Y 2019 *Nature* **572** 624
[17] Dagotto E, Hotta T and Moreo A 2001 *Phys. Rep.* **344** 1
[18] Imada M, Fujimori A and Tokura Y 1998 *Rev. Mod. Phys.* **70** 1039
[19] Dong S, Liu J M, Cheong S W and Ren Z F 2015 *Adv. Phys.* **64** 519
[20] Rau J G, Lee E K H and Kee H Y 2016 *Annu. Rev. Condens. Matter Phys.* **7** 195
[21] Lu C L and Liu J M 2020 *Adv. Mater.* **32** 1904508
[22] Dagotto E 2005 *Science* **309** 257
[23] Zubko P, Gariglio S, Gabay M, Ghosez P and Triscone J M 2011 *Annu. Rev. Condens. Matter Phys.* **2** 141
[24] Syono Y, Akimoto S I and Kohn K 1969 *J. Phys. Soc. Jpn.* **26** 993
[25] Chmaissem O, Dabrowski B, Kolesnik S, Mais J, Brown D E, Kruk R, Prior P, Pyles B and Jorgensen J D 2001 *Phys. Rev. B* **64** 134412
[26] Battle P D, Gibb T C and Jones C W 1988 *J. Solid State Chem.* **74** 60
[27] Belik A A, Matsushita Y, Katsuya Y, Tanaka M, Kolodiazhnyi T, Isobe M and Takayama-Muromachi E 2011 *Phys. Rev. B* **84** 094438
[28] Søndenå R, Ravindran P, Stølen S, Grande T and Han-fland M 2006 *Phys. Rev. B* **74** 144102
[29] Nielsen M B, Ceresoli D, Parisiades P, Prakapenka V B, Yu T, Wang Y B and Bremholm M 2014 *Phys. Rev. B* **90** 214101
[30] Song R N, Hu M H, Chen X R and Guo J D 2015 *Front. Phys.* **10** 321
[31] Mandal P, Hassen A and Loidl A 2004 *Phys. Rev. B* **69** 224418
[32] Sakai H, Ishiwata S, Okuyama D, Nakao A, Nakao H, Murakami Y, Taguchi Y and Tokura Y 2010 *Phys. Rev. B* **82** 180409
[33] Aich P, Meneghini C, Tortora L, Siruguri V, Kaushik S D, Fu D and Ray S 2019 *J. Mater. Chem. C* **7** 3560
[34] Blöchl P E, Jepsen O and Andersen O K 1994 *Phys. Rev. B* **49** 16223
[35] Kresse G and Joubert D 1999 *Phys. Rev. B* **59** 1758
[36] Perdew J P, Ruzsinszky A, Csonka G I, Vydrov O A, Scuseria G E, Constantin L A, Zhou X and Burke K 2008 *Phys. Rev. Lett.* **100** 136406
[37] Dudarev S L, Botton G A, Savrasov S Y, Humphreys C J and Sutton A P 1998 *Phys. Rev. B* **57** 1505
[38] Søndenå R, Stølen S, Ravindran P, Grande T and Allan N L 2007 *Phys. Rev. B* **75** 184105
[39] Daoud-Aladine A, Martin C, Chapon L C, Hervieu M, Knight K S, Brunelli M and Radaelli P G 2007 *Phys. Rev. B* **75** 104417
[40] Meskine H, Saha-Dasgupta T and Satpathy S 2004 *Phys. Rev. Lett.* **92** 056401